Research in Astron. Astrophys. **2013** Vol. **13** No. **10**, 1163–1180
http://www.raa-journal.org *http://www.iop.org/journals/raa*

Research in Astronomy and Astrophysics

A disk-corona model for the low/hard state of black hole X-ray binaries *

Jiu-Zhou Wang, Ding-Xiong Wang and Chang-Yin Huang

School of Physics, Huazhong University of Science and Technology, Wuhan 430074, China; *dxwang@mail.hust.edu.cn*

Received 2013 January 9; accepted 2013 May 17

Abstract A disk-corona model for fitting the low/hard (LH) state of the associated steady jet in black hole X-ray binaries (BHXBs) is proposed based on the large-scale magnetic field configuration that arises from the coexistence of the Blandford-Znajek (BZ) and Blandford-Payne (BP) processes, where the magnetic field configuration for the BP process is determined by the requirement of energy conversion from Poynting energy flux into kinetic energy flux in the jet. It is found that corona current is crucial to guarantee the consistency of the jet launching from the accretion disk. The relative importance of the BZ and BP processes in powering jets from black hole accretion disks is discussed, and the LH state of several BHXBs is fitted based on our model. In addition, we suggest that magnetic field configuration can be regarded as the second parameter for governing the state transition of BHXBs.

Key words: accretion, accretion disks — black hole physics — magnetic field — jet power

1 INTRODUCTION

Spectral states observed in black hole X-ray binaries (BHXBs) involve a number of unresolved issues in astrophysics and display complex variations not only in their luminosities and energy spectra, but also in the presence/absence of jets and quasi-periodic oscillations (QPOs). Not long ago, McClintock & Remillard (2006, hereafter MR06) used four parameters to define X-ray states based on the very extensive RXTE data archive for BHXBs, in which three states, i.e., thermal dominant state, low/hard (LH) state and steep power law state, are included. Although a consensus on classification of spectral states of BHXBs has not been reached, it is widely accepted that these states can be reduced to only two basic states, i.e., a hard state and a soft one, and jets can be observed in hard states, but cannot be in soft states.

The accretion flow in LH state is usually supposed to be a truncated thin disk with an inner advection-dominated accretion flow (ADAF) in the prevailing scenario (Esin et al. 1997, 1998; MR06; Done et al. 2007). Generally speaking, the thermal component of the spectra of BHXBs can be well fitted by a truncated thin accretion disk, while the power law component can be interpreted by an ADAF. Although the X-ray, EUV and UV spectra of XTE J1118+480 can be satisfactorily explained by a truncated thin disk plus an ADAF (Esin et al. 2001), the IR fluxes are significantly underestimated and the radio emission cannot be interpreted. Yuan et al. (2005) fitted the spectrum of

* Supported by the National Natural Science Foundation of China.

XTE J1118+480, and proposed a coupled accretion-jet model to interpret the observations, in which the jet dominates the radio and infrared emission, the thin disk dominates the UV emission, and the hot flow produces most of the X-ray emission. This model successfully fits the multiwavelength spectrum of the source, and further testing of this model can be seen in Zhang et al. (2010).

An ADAF plus a truncated thin disk has become the major model used in interpreting spectra of BHXBs in LH state; however, recent observations show some contradiction with it. For example, *XMM-Netwon* observations of GX 339-4 show that a broad iron line together with a dim, hot thermal component was present in its spectra during the hard state. This effect seems to be observed in a few other sources such as Cygnus X-1 and SWIFT J1753.5-0127 (Miller et al. 2006a,b). Recently, Reis et al. (2009) studied the *Chandra* observation of XTE J1118+480 in the canonical LH state, and a thermal disk emission with a temperature of approximately 0.21 keV was found at greater than the 14σ confidence level. They concluded that this thermal emission most likely originated from an accretion disk extending close to the innermost stable circular orbit (ISCO). The results of fits made to both components (thermal component and broad iron line) strongly suggest that a standard thin disk remains at or near the ISCO, at least in bright phases of the LH state.

In order to interpret the thermal component and broad iron line in the luminous LH state, some authors suggested that the accretion geometry could be described as a cool inner disk and an even cooler outer disk, separated by a gap filled with an ADAF (Mayer & Pringle 2007; Liu et al. 2007).

Recently, Reis et al. (2010) presented an X-ray study of eight black holes (BHs) in the LH state, and they found that a thermal disk continuum with a color temperature consistent with $L \propto T^4$ was clearly detected in all eight sources and the detailed fits to the line profiles excluded a truncated disk in each case.

Besides the dominant power-law component, another feature of the LH state of BHXBs is its association with quasi-steady jets. Although the ADAF model is successful in fitting the spectra of the LH state of some BHXBs, the details of how associated jets are produced have not been addressed.

Different mechanisms have been proposed to interpret the jet production in BH systems of different scales, such as the plasma gun (Contopoulos 1995), the cosmic battery (Contopoulos & Kazanas 1998) and the magnetic tower (Lynden-Bell 1996). The most promising mechanisms for powering jets are Blandford-Znajek (BZ) and Blandford-Payne (BP) processes, which rely on a poloidal, large-scale magnetic field anchored on an accretion disk around a spinning BH (Blandford & Znajek 1977; Blandford & Payne 1982, hereafter BP82; Livio 2002; Doeleman et al. 2012; for a review see Spruit 2010).

In this paper, we intend to model the LH state of BHXBs based on a disk-corona model, in which the inner edge of the accretion disk is assumed to extend to ISCO, and the jets are driven by the large-scale open magnetic field that arises from the coexistence of the BZ and BP processes. This paper is organized as follows. In Section 2, based on the energy conversion from Poynting energy flux into the kinetic energy flux in the jet, we argue that some current within the corona is required to flow across the magnetic surfaces, which are formed due to the rotation of the open field lines anchored at the accretion disk. Henceforth, the current is referred to as corona current. In Section 3, we propose a configuration for the magnetic field that arises from the coexistence of the BZ and BP processes based on the energy conversion in the jet, and discuss the relative importance of these two mechanisms in driving jets from BH systems. In Section 4, the spectral profiles of the LH state of four BHXBs are fitted based on our model, and the relation between jet power and X-ray luminosity is checked by adjusting accretion rate and the outer boundary of the BP magnetic field configuration. Finally, in Section 5, we discuss some issues related to our model. We propose a scenario of state transitions from the LH state to the very high (VH) state, and suggest that the magnetic field configuration could be regarded as the second parameter in state transitions experienced by BHXBs.

Throughout this paper, the geometric units $G = c = 1$ are used.

2 CONVERSION OF ENERGY IN JETS AND CORONA CURRENT

Both matter outflow and Poynting flux are produced via the large-scale magnetic field anchored on the disk around a rotating BH. What is the relation between the two kinds of fluxes? As shown in Figure 1, Poynting flux $\boldsymbol{S}_{\rm E}^{\rm P} = \boldsymbol{E}^{\rm P} \times \boldsymbol{B}^{\varphi}$ is produced by the magnetic field lines dragged by the rotating disk, where $\boldsymbol{E}^{\rm P}$ is the poloidal induced electric field, and $\boldsymbol{B}^{\varphi}$ is the toroidal magnetic field. Obviously, both $\boldsymbol{E}^{\rm P}$ and $\boldsymbol{B}^{\varphi}$ arise from disk rotation, and they are expressed as follows,

$$\boldsymbol{E}^{\rm P} = -\boldsymbol{v}^{\rm F} \times \boldsymbol{B}^{\rm P}, \tag{1}$$

$$\boldsymbol{S}_{\rm E}^{\rm P} = \boldsymbol{E}^{\rm P} \times \boldsymbol{B}^{\varphi}, \tag{2}$$

where $\boldsymbol{S}_{\rm E}^{\rm P}$ is the poloidal Poynting flux along the field line.

According to BP82, the conservation of energy and angular momentum along each field line can be written as follows,

$$e = e_{\rm matter} + e_{\rm Poynting} = {\rm const}\,, \tag{3}$$

$$l = l_{\rm matter} + l_{\rm Poynting} = {\rm const}\,. \tag{4}$$

The quantities $e_{\rm matter}$ and $e_{\rm Poynting}$ are specific energies of matter and the electromagnetic (EM) field, respectively, and they read as (BP82)

$$\begin{cases} e_{\rm matter} = v^2/2 + h + \Phi, \\ e_{\rm Poynting} = -\omega r B^{\varphi}/k\,, \end{cases} \tag{5}$$

where r is the cylindrical radius of the field line, and ω is the angular velocity of the field line, which is equal to the angular velocity of the disk $\Omega_{\rm d} = \frac{1}{M(\chi^3+a_*)}$ at the radius of the footpoint $r_{\rm d} = M\chi^2$. The quantities $l_{\rm matter}$ and $l_{\rm Poynting}$ are respectively specific angular momenta of matter and the EM field, and they read as

$$\begin{cases} l_{\rm matter} = r v^{\varphi}, \\ l_{\rm Poynting} = -r B^{\varphi}/k\,, \end{cases} \tag{6}$$

where the quantities h, Φ and $-\omega r B^{\varphi}/k$ in Equation (5) are specific enthalpy, gravitational potential, and the work done on the streaming gas by the magnetic torque, respectively. The quantity $-rB^{\varphi}/k$

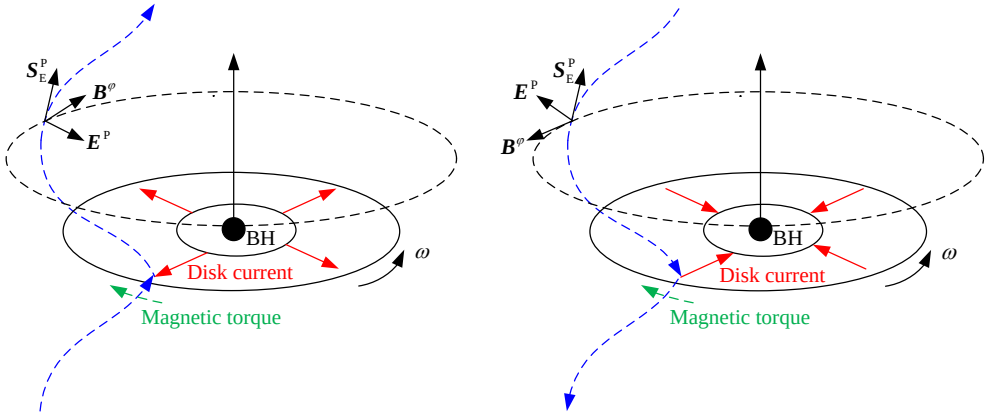

Fig. 1 Poynting flux is driven by a rotating disk around a BH via magnetic torque exerted on the disk current. The green arrow represents the direction of magnetic torque, and the red solid and the blue dashed arrows represent disk current and magnetic field lines, respectively.

in Equation (6) represents the impulse of the magnetic torque, and the parameter k is related to the ratio of the mass flux to the magnetic flux for each magnetic field line as follows,

$$k/4\pi \equiv \rho v^{\rm P}/B^{\rm P}\,. \tag{7}$$

The meanings of $e_{\rm Poynting}$ and $l_{\rm Poynting}$ can be clarified more clearly as follows. The poloidal flux of EM angular momentum can be written as $S_{\rm L}^{\rm P} = -rB^{\varphi}B^{\rm P}/4\pi = -rB^{\varphi}\rho v^{\rm P}/k$ (MacDonald & Thorne 1982), thus we have

$$\begin{cases} \frac{S_{\rm L}^{\rm P}}{\rho v^{\rm P}} = -rB^{\varphi}/k = l_{\rm Poynting}\,, \\ \frac{S_{\rm E}^{\rm P}}{\rho v^{\rm P}} = -\omega rB^{\varphi}/k = e_{\rm Poynting}\,. \end{cases} \tag{8}$$

We conclude that $e_{\rm Poynting}$ and $l_{\rm Poynting}$ are respectively EM specific energy and angular momentum corresponding to mass flux. Based on Amperes law we have

$$\oint \boldsymbol{B}\cdot d\boldsymbol{l} = 2\pi rB^{\varphi} = 4\pi\sum I\,. \tag{9}$$

As shown in Equation (8), $e_{\rm Poynting}$ is proportional to rB^{φ}. Considering that $e_{\rm Poynting}$ is continuously converted to kinetic energy in the jet (BP82; Spruit 1996, 2010), we infer that the absolute values of both rB^{φ} and $\sum I$ in Equation (9) must continuously decrease along the jet, where $\sum I$ is the algebraic sum of current flowing inside the magnetic surface formed due to the rotation of the field line.

In the standard model for the jet launched by magneto-centrifugal acceleration, there are three distinct regions as shown in Figure 2 (Bisnovatyi-Kogan & Ruzmaikin 1976, BP82; Spruit 1996, 2010).

In the atmosphere of the disk up to the Alfvén surface, the magnetic field dominates over gas pressure and kinetic energy of the outflow, and the outflow experiences a centrifugal force accelerating along the field lines in this region which is force free. On the other hand, the corona is a perfect launching site for outflow from the accretion disk (Merloni & Fabian 2002), and the disk-corona model provides a possible scenario for interpreting the LH state associated with a quasi-steady jet

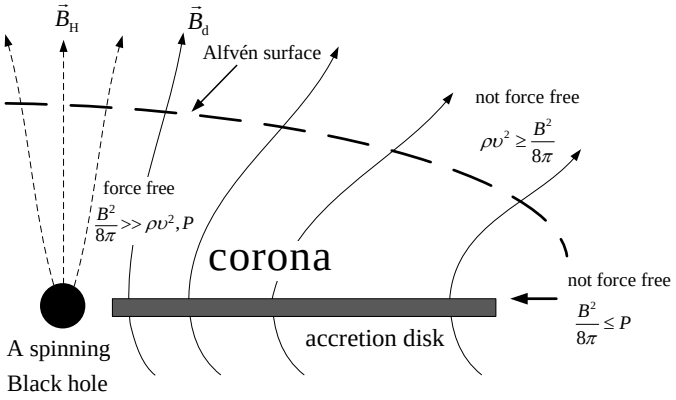

Fig. 2 Three regions in a magnetically accelerated flow from an accretion disk. The corona is assumed to exist between the disk surface and the Alfvén surface indicated by the thick dashed line. $B_{\rm H}$ (*thin dashed lines*) and $B_{\rm d}$ (*thin solid lines*) represent the poloidal magnetic field on the BH horizon and disk, respectively.

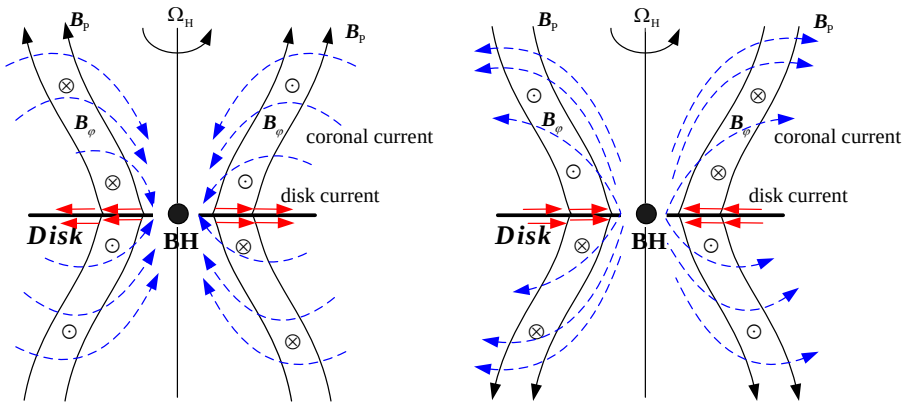

Fig. 3 A schematic drawing of corona current flowing across the magnetic surface, where disk and corona currents are represented respectively by red solid and blue dashed arrows. The symbols $\odot$ and $\otimes$ represent the outward and inward toroidal magnetic field lines, respectively.

from BHXBs. From the above discussion, we infer that corona current must flow across the magnetic surfaces as shown in Figure 3, and it can be expressed from Equation (9) as follows,

$$I_{\rm cor}(r) = rB^{\varphi}/2\,, \tag{10}$$

where $I_{\rm cor}(r)$ is the corona current threading the magnetic surface above the cylindrical radius r. Inspecting Figure 3, we find that corona current is essential for interpreting energy conversion in the jet.

There are two puzzles related to corona current. The first one is whether the corona current can flow across the magnetic surface in the region with centrifugal acceleration, where $B^2/8\pi \gg \rho v^2$ is required as shown in Figure 2. In fact, the condition for centrifugal acceleration does not imply no current is flowing across the magnetic surface. Inspecting Figures 1 and 3, we find that the corona current is required by the continuity of the current flowing in the disk, and it is driven by the induced electric field $\boldsymbol{E}^{\rm P}$ or the electric potential difference between the two adjacent magnetic surfaces.

The second puzzle is that the quantity $-\omega rB^{\varphi}/k$ appears to have two different meanings, i.e., (i) the work done on the streaming gas by the magnetic torque (BP82), and (ii) EM specific energy $e_{\rm Poynting}$ along a field line given by Equation (8). How can we understand the process where the work done by the magnetic torque continuously decreases during the energy conversion in the jet? This puzzle can be easily resolved by invoking corona current. The work done by the magnetic torque consists of two parts, one is on the disk current, and the other one is on the corona current. From Figure 3 we find that the two works done by the magnetic torque have opposite signs, because the direction of the disk current is opposite to that of the corona current. The total work by the magnetic torque is the integral of the differential work from the neutral plane at $z = 0$ to the Alfvén surface. So the work is zero at $z = 0$ for $B^{\varphi} = 0$, and it attains its maximum at the disk surface, and then it decreases along the jet due to the negative work on the corona current. It is the work done on the corona current by the magnetic torque that gives rise to the conversion of EM energy into kinetic energy in the jet.

Thus we conclude that the corona current is not only required by the continuity of the disk current but is also essential for understanding energy conversion in the jet. In addition, we can estimate the efficiency of the conversion from EM energy into kinetic energy in the jet in terms of rB^{φ}. The conversion efficiency can be defined as the ratio of $e_{\rm matter,A}$ to e, which are the specific

energy of matter at the Alfvén surface and the total specific energy along a field line, respectively. Thus we have conversion efficiency that can be expressed as

$$\begin{aligned}\eta_{\rm E} &\equiv e_{\rm matter,A}/e = (e - e_{\rm matter,A})/e \\ &\simeq 1 - e_{\rm matter,A}/e_{\rm matter,d} = 1 - (rB^{\varphi})_{\rm A}/(rB^{\varphi})_{\rm d}, \end{aligned} \tag{11}$$

where $e_{\rm matter,d}$ and $e_{\rm matter,A}$ are the EM specific energy at the disk surface and Alfvén surface, respectively. In deriving the above equation, $e_{\rm matter,d} \simeq e$ is assumed, since EM specific energy is dominant at the disk surface.

Thus, we infer that the conversion efficiency depends on the variation of rB^{φ} along the field line. For example, we have about $1/3$ of the EM energy converted into kinetic energy in the jet for the ratio $(rB^{\varphi})_{\rm A}/(rB^{\varphi})_{\rm d} = 2/3$.

3 MAGNETIC FIELD CONFIGURATION BASED ON ENERGY CONVERSION

We can constrain the magnetic field configuration in the accretion disk based on the energy conversion in the jet. The power of the magnetic torque on the radial disk current between the two adjacent magnetic surfaces is

$$d{\rm P}_{\rm d} = B_{\rm d}^{\rm P}\Omega_{\rm d} I_{\rm d} r_{\rm d} dr_{\rm d}\,, \tag{12}$$

where the subscript 'd' indicates the quantities at the disk surface. On the other hand, the work done on the streaming gas per unit mass at the cylindrical radius r is

$$W_{\rm line}(r) = -\omega r B^{\varphi}/k = 2\omega I_{\rm cor}(r)/k\,. \tag{13}$$

Combining Equation (10) with (13), and considering $\omega = \Omega_{\rm d}$, we have

$$d{\rm P}_{\rm d} = W_{\rm line}(r_{\rm d})\dot{M}_{\rm jet} dr_{\rm d} = (2\omega I_{\rm cor}(r_{\rm d})/k)\dot{M}_{\rm jet} dr_{\rm d}\,, \tag{14}$$

where $\dot{M}_{\rm jet}$ is the mass outflow rate in a jet of unit width, which is expressed in Equation (17).

Considering the continuity of the corona current and disk current, we have $I_{\rm cor}(r_{\rm d}) = I_{\rm d}(r_{\rm d})$. Uniting Equations (12) and (14), we have the relation between mass loss rate at $r_{\rm d}$ and the poloidal magnetic field $B_{\rm d}^{\rm P}$ as follows,

$$\dot{M}_{\rm jet}(r_{\rm d}) = B_{\rm d}^{\rm P} r_{\rm d} k/2\,. \tag{15}$$

Following Blandford & Begelman (1999), we have accretion rate $\dot{M}$ varying with the disk radius as follows,

$$\dot{M} = \dot{M}_{\rm in}(r_{\rm d}/r_{\rm in})^{s}, \qquad 0 < s < 1\,, \tag{16}$$

where $\dot{M}_{\rm in}$ is the accretion rate at the inner edge of the disk, which is related to Eddington luminosity by $\dot{M}_{\rm in} = \dot{m}_{\rm in} L_{\rm Edd}/(0.1c^2)$. Henceforth, the subscript 'in' indicates the quantities at the inner edge of the accretion disk. The mass outflow rate in the jet is given by

$$\dot{M}_{\rm jet}(r_{\rm d}) = d\dot{M}/dr_{\rm d} = \dot{M}_{\rm in}(s/r_{\rm in})(r_{\rm d}/r_{\rm in})^{s-1}\,. \tag{17}$$

Combining Equations (15) and (17), we have the relation between poloidal magnetic field at the disk surface and $\dot{M}_{\rm in}$ as follows,

$$B_{\rm d}^{\rm P}(r_{\rm d}) = \dot{M}_{\rm in}(2s/kr_{\rm in}^2)(r_{\rm d}/r_{\rm in})^{s-2}\,. \tag{18}$$

The poloidal magnetic field far from the disk surface is assumed to be roughly self-similar, and is given as (BP82, Lubow et al. 1994),

$$B^{\rm P}(r_{\rm d}, \varsigma) = B_{\rm d}^{\rm P}(r_{\rm d})\varsigma^{-\alpha}\,, \tag{19}$$

where $\varsigma \equiv (r/r_{\rm d})$ is the cylindrical radius of the field line. Considering Equations (18) and (19), we have the 3-D axisymmetric magnetic field distribution on the accretion disk as follows,

$$B_{\rm d}^{\rm P}(r_{\rm d},\varsigma) = B_{\rm in}(r_{\rm d}/r_{\rm in})^{s-2}\varsigma^{-\alpha}\,, \tag{20}$$

where $B_{\rm in}$ is the poloidal magnetic field at the inner edge of the disk.

The strength of the magnetic field on the BH horizon can be determined based on the balance between the magnetic pressure on the horizon and the ram pressure of the innermost parts of an accretion as follows (Moderski et al. 1997),

$$B_{\rm H}^2/(8\pi) = P_{\rm ram} \sim \rho c^2 \sim \dot{M}_{\rm in}/(4\pi r_{\rm H}^2)\,. \tag{21}$$

Equation (21) can be rewritten as

$$\dot{M}_{\rm in} = \alpha_{\rm m} B_{\rm H}^2 r_{\rm H}^2 = \alpha_{\rm m}(1+q)^2 B_{\rm H}^2 M^2\,, \tag{22}$$

where $r_{\rm H} \equiv M(1+q)$ is the radius of the BH horizon, and $q \equiv \sqrt{1-a_*^2}$ is a function of BH spin, and the parameter $\alpha_{\rm m}$ is adjustable due to the uncertainty in Equation (22).

The optimal BZ power is given by Equation (23) as a function of BH spin (Lee et al. 2000; Wang et al. 2002), and the BP power is given by Equation (24) as an integral over the region with a large-scale open magnetic field from the inner edge to the outer boundary (Cao 2002, hereafter C02).

$$\begin{cases} P_{\rm BZ} = B_{\rm H}^2 M^2 Q^{-1}(\arctan Q - a_*/2) \\ Q \equiv \sqrt{(1-q)/(1+q)} \end{cases}\,, \tag{23}$$

$$P_{\rm BP} = \int_{r_{\rm in}}^{r_{\rm out}} (\gamma_{\rm j}-1)\dot{M}_{\rm jet} dr_{\rm d} = \dot{M}_{\rm in} s \int_1^{\xi_{\rm out}} (\gamma_{\rm j}-1)\xi^{s-1} d\xi\,, \tag{24}$$

where $\xi_{\rm out} \equiv r_{\rm out}/r_{\rm in}$ is the radius of the outer boundary of the large scale open magnetic field in terms of $r_{\rm in}$. The parameter $\gamma_{\rm j} \equiv (1-v_{\rm A}^2)^{-1/2}$ is the Lorentz factor of the outflow at the Alfvén surface, and it is related to the parameters $\alpha_{\rm m}, s, a_*$ and α by

$$\frac{\xi^{s-2}\chi_{\rm in}^4}{\alpha_{\rm m} s(1+q)^2}\left(\frac{\xi\chi_{\rm in}^2}{\xi^{3/2}\chi_{\rm in}^3 + a_*}\right)^{\alpha} = \gamma_{\rm j}^{-\alpha}(\gamma_{\rm j}^2-1)^{(\alpha+1)/2}\,, \tag{25}$$

where $\chi_{\rm in}$ is defined as $\chi_{\rm in} \equiv \sqrt{r_{\rm in}/M}$. The derivation of Equation (25) is given in the Appendix.

The relative importance of the BZ and BP processes can be estimated by combining Equations (23), (24) and (22) based on the magnetic field configuration given in Figure 1, and the ratio of the BZ to BP powers is

$$P_{\rm BZ}/P_{\rm BP} = \frac{Q^{-1}(\arctan Q - a_*/2)}{\alpha_{\rm m}(1+q)^2 s\int_1^{\xi_{\rm out}}(\gamma_{\rm j}-1)\xi^{s-1}d\xi}\,. \tag{26}$$

Four parameters ($\alpha_{\rm m}$, a_*, s and α) are involved in Equation (26), and $r_{\rm out} = 1000M$ is fixed in the calculations. By using Equation (26) we have the contours of the ratio of $P_{\rm BZ}$ to $P_{\rm BP}$ in $\alpha - s$ parameter space with different values of $\alpha_{\rm m}$ and a_* as shown in Figure 4.

Inspecting Figure 4, we find that the ratio of $P_{\rm BZ}$ to $P_{\rm BP}$ is less than or around unity for $0 < s < 0.12$, and $2 < \alpha \leq 5$ with $\alpha_{\rm m} = 0.1, 1$. It implies that the BZ power is not dominant over the BP power for the large outer boundary of the open magnetic field on the disk, $r_{\rm out} = 1000M$, except for the case of extreme BH spin $a_* \to 0.998$ with $\alpha \sim 5$, and this result is in accordance with those obtained by other authors (e.g., Ghosh & Abramowicz 1997; Livio et al. 1999; Meier 1999).

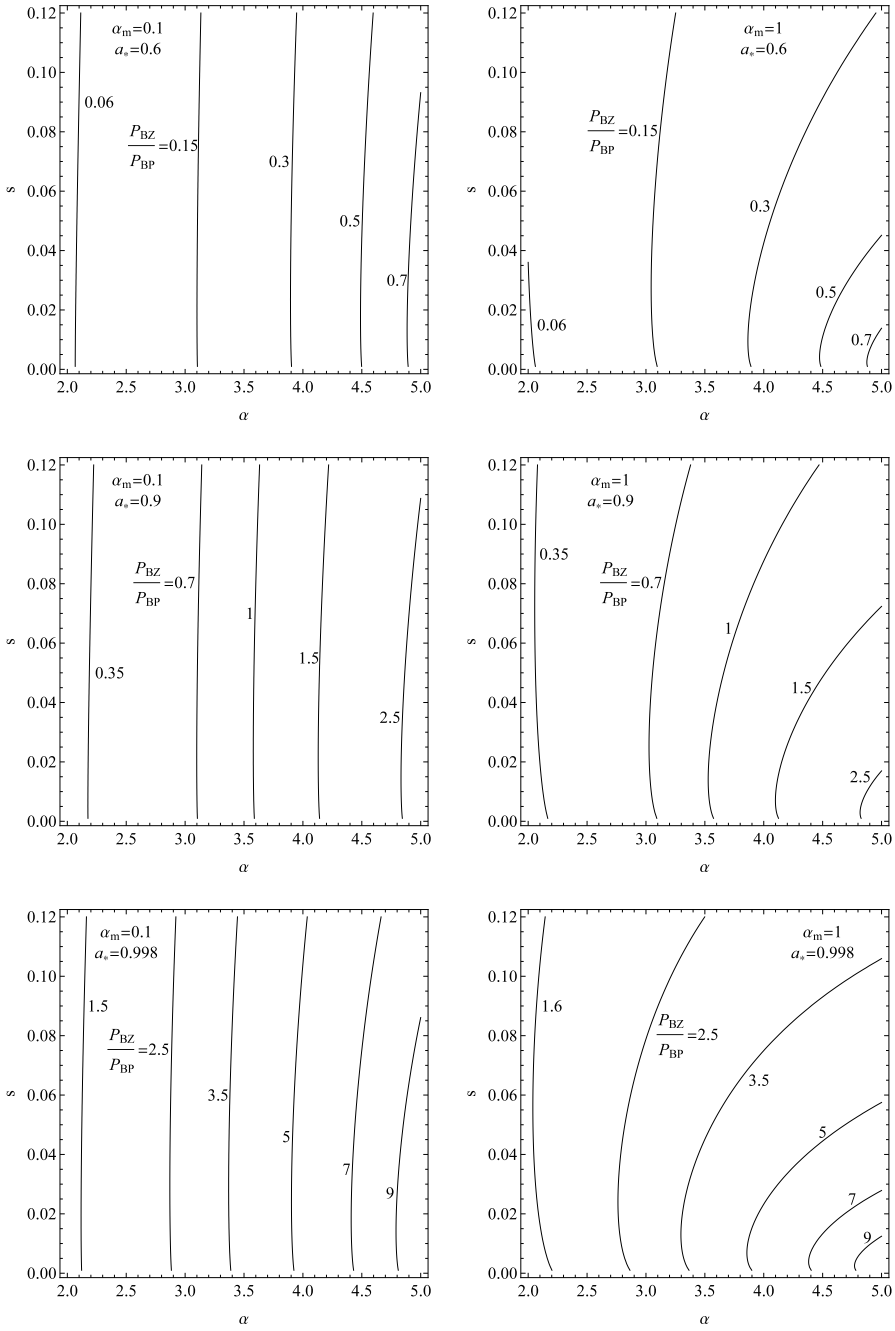

Fig. 4 The contours of the ratio of $P_{\rm BZ}$ to $P_{\rm BP}$ in α – s parameter space with different values of $\alpha_{\rm m}$ and a_*.

4 FITTING THE LH STATE OF FOUR BHXBS

In this section we intend to fit the LH state associated with quasi-steady jets of four BHXBs, XTE J1550564, GRO J165540, GRS 1915+105 and 4U 154347. The jet power is regarded as the sum of

the BZ and BP powers, i.e.,

$$P_{\rm jet} = P_{\rm BZ} + P_{\rm BP}\,. \tag{27}$$

In addition, we discuss the constraints of the relation between jet power and X-ray luminosity on the variation of $\dot{m}_{\rm in}$ and $r_{\rm out}$ in the state transition of BHXBs.

4.1 Effect of Launching a Jet from the Accretion Disk on Energy and Angular Momentum

The fitting of the LH state is given based on the conservation of energy and angular momentum by considering the launching of a jet from the accretion disk. Following C02, the kinetic flux of the jet can be written as

$$F_{\rm jet} = \dot{m}_{\rm jet}(\gamma_{\rm j} - 1)\,. \tag{28}$$

Considering that Poynting flux is much larger than kinetic flux near the disk surface, we can relate $F_{\rm jet}$ at the Alfvén surface to the Poynting flux at the disk surface as follows,

$$S_{\rm E}^{\rm P} = 3F_{\rm jet}\,, \tag{29}$$

where the factor '3' in Equation (29) implies that one third of the energy in the Poynting flux is assumed to be converted into kinetic energy of the jet.

As is well known, the angular momentum flux $S_{\rm L}^{\rm P}$ extracted electromagnetically from the disk surface is related to the Poynting energy flux as follows,

$$S_{\rm L}^{\rm P} = S_{\rm E}^{\rm P}/\Omega_{\rm d}\,. \tag{30}$$

Combining Equations (28)–(30), we have

$$S_{\rm L}^{\rm P} = 3\dot{m}_{\rm jet}(\gamma_{\rm j} - 1)/\Omega_{\rm d}\,, \tag{31}$$

where $\dot{m}_{\rm jet} \equiv \dot{M}_{\rm jet}/4\pi r_{\rm d}$ is the mass loss rate per unit area at the footpoint of the jet.

The integrated shear stress of the disk should be affected by the transport of angular momentum and energy in the jet, resulting in a decrease in the dissipation of the disk and radiation from it. When the jet occurs, the conservation equations of energy and angular momentum can be written as

$$\frac{d}{dr_{\rm d}}(\dot{M}_{\rm d}E^{\dagger} - T_{\rm visc}\Omega_{\rm d}) \;=\; 4\pi r_{\rm d}[(\dot{m}_{\rm jet} + F_{\rm rad})E^{\dagger} + S_{\rm L}^{\rm P}\Omega_{\rm d}], \tag{32}$$

$$\frac{d}{dr_{\rm d}}(\dot{M}_{\rm d}L^{\dagger} - T_{\rm visc}) \;=\; 4\pi r_{\rm d}[(\dot{m}_{\rm jet} + F_{\rm rad})L^{\dagger} + S_{\rm L}^{\rm P}], \tag{33}$$

where $T_{\rm visc}$ and $F_{\rm rad}$ are respectively the internal viscous torque and the energy flux radiated away from the surface of the disk; $E^{\dagger}$ and $L^{\dagger}$ are respectively specific energy and angular momentum of the disk matter, which is expressed by (Novikov & Thorne 1973)

$$E^{\dagger} \;=\; (1 - 2\chi^{-2} + a_*\chi^{-3})/(1 - 3\chi^{-2} + 2a_*\chi^{-3})^{1/2}, \tag{34}$$

$$L^{\dagger} \;=\; M\chi(1 - 2a_*\chi^{-3} + a_*^2\chi^{-4})/(1 - 3\chi^{-2} + 2a_*\chi^{-3})^{1/2}, \tag{35}$$

where $\chi \equiv \sqrt{r_{\rm d}/M} = \xi^{1/2}\chi_{\rm in}$, and the quantities $E^{\dagger}$ and $L^{\dagger}$ are related by

$$dE^{\dagger}/dr_{\rm d} = \Omega_{\rm d}dL^{\dagger}/dr_{\rm d}\,. \tag{36}$$

Combining Equations (32), (33) and (36), we have the radiation flux from the disk as follows,

$$\begin{aligned} F_{\rm rad}(r_{\rm d}) \;=\; & -\frac{d\Omega_{\rm d}/dr_{\rm d}}{4\pi r_{\rm d}}(E^{\dagger} - \Omega_{\rm d}L^{\dagger})^{-2} \times \Big(\int_{r_{\rm in}}^{r_{\rm d}} (E^{\dagger} - \Omega_{\rm d}L^{\dagger})\dot{M}\frac{dL^{\dagger}}{dr_{\rm d}}dr_{\rm d} \\ & + (E_{\rm in}^{\dagger} - \Omega_{\rm d,in}L_{\rm in}^{\dagger})T_{\rm in} - \int_{r_{\rm in}}^{r_{\rm d}} (E^{\dagger} - \Omega_{\rm d}L^{\dagger})4\pi r_{\rm d}S_{\rm L}^{\rm P}dr_{\rm d}\Big), \end{aligned} \tag{37}$$

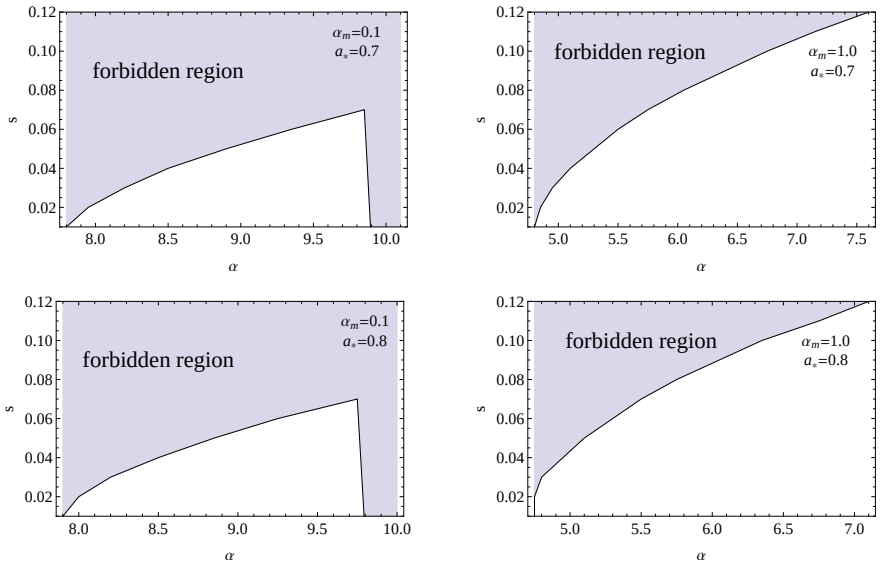

Fig. 5 The contour of $F_{\rm rad}(r_{\rm d})=0$ for different values of a_* and $\alpha_{\rm m}$ in $s-\alpha$ parameter space, in which $F_{\rm rad}(r_{\rm d})$ becomes negative in the forbidden region.

where $E^{\dagger}_{\rm in}$, $L^{\dagger}_{\rm in}$, $\Omega_{\rm d,in}$ and $T_{\rm in}$ in Equation (37) are respectively specific energy, specific angular momentum, angular velocity and torque at the inner edge of the accretion disk.

Inspecting Equation (37), we find that the jet launched from the accretion disk does result in a negative contribution to the disk radiation, which is represented by the term related to the angular momentum flux $S^{\rm P}_{\rm L}$. Thus, we think that the lunching of a jet from the accretion disk is indeed essential for interpreting the association of the LH state with the quasi-steady jet in BHXBs.

Furthermore, we obtain a rather tight constraint on the parameters s, α, $\alpha_{\rm m}$ and $\dot{m}_{\rm in}$, which are involved in our model based on the following arguments.

(i) The contour of $F_{\rm rad}(r_{\rm d})=0$ can be plotted in $\alpha-s$ parameter space by using Equation (37) as shown in Figure 5, in which $F_{\rm rad}(r_{\rm d})$ becomes negative in the forbidden region.

(ii) The Lorentz factor in the BP process, $\gamma_{\rm j}$, can be calculated in our model (see Eq. (25) and Appendix for details), and the curves of $\gamma_{\rm j}$ varying with disk radius for different values of α, $\alpha_{\rm m}$ and s are shown in Figure 6. On the other hand, the Lorentz factor $\Gamma_{\rm j}$ in the LH state should be no greater than 2 (Fender et al. 2004, hereafter FBG04). Considering that the jet is driven by the BZ and BP processes in our model, and the Lorentz factor of the BZ jet is generally greater than that of the BP jet, we have $\gamma_{\rm j}<\Gamma_{\rm j}\leq 2$. From Figure 6 we conclude that the parameter α should be no less than 5, i.e., $\alpha\geq 5$.

Inspecting Figure 5, we have the constraint of positive disk radiation on the parameters, α, $\alpha_{\rm m}$, and s, i.e., $4.5<\alpha<7$, $\alpha_{\rm m}=1$ and a small s, such as $s\approx 0.01\sim 0.02$.

Inspecting Figure 6, we have the constraint of the Lorentz factor on the parameters α, $\alpha_{\rm m}$ and s, i.e., $\alpha\geq 5$, $\alpha_{\rm m}=1$ and $0.01<s<0.1$.

Combining the above results, we can select the values of these parameters in the set ($\alpha_{\rm m}=1, \alpha=5, s=0.02$) or ($\alpha_{\rm m}=1, \alpha=5, s=0.01$) in fitting the LH states with a steady jet from the four BHXBs as shown in Table 1.

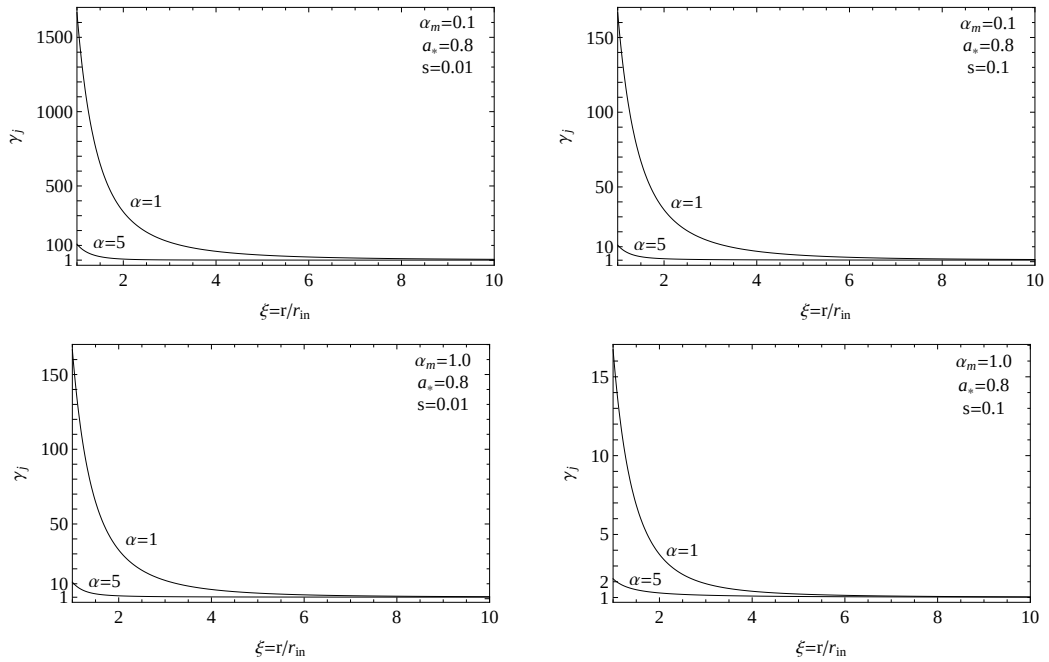

Fig. 6 The curves of Lorentz factor $\gamma_{\rm j}$ versus disk radius $\xi \equiv r_{\rm d}/r_{\rm in}$ for different values of s and $\alpha_{\rm m}$.

Table 1 Input and Fitting Parameters of the LH State of Four BHXBs

BHXBs	Input parameters				Fitting parameters			
	a_*	M ($M_\odot$)	D (kpc)	i (°)	$\dot{m}_{\rm in}$	α	$\alpha_{\rm m}$	s
XTE J1550-564	0.34	9.10	4.38	74.7	0.032	5	1.0	0.01
GRO J1655-40	0.7	6.30	3.2	70.2	0.035	5	1.0	0.02
GRS 1915+105	0.975	14.0	11.0	66.0	0.200	5	1.0	0.02
4U 1543-475	0.8	9.4	7.5	20.7	0.005	5	1.0	0.02

4.2 Fitting Spectral Profiles of the LH State of BHXBs

The spectra of the LH state are fitted based on the disk-corona model given by Gan et al. (2009, hereafter GWL09). This model is different from GWL09 in three aspects. (i) The magnetic field configuration consists of large-scale open field lines threading the BH horizon and accretion disk as shown in Figure 2, while that in GWL09 consists of large-scale closed field lines connecting the BH horizon and the inner disk. (ii) The BZ and BP mechanisms are invoked respectively to drive jets from a spinning BH and its surrounding accretion disk, and energy is extracted respectively from the BH and the inner disk, and channeled away. However, in GWL09, we have no open magnetic field for launching a jet, and energy is transferred from the BH into the inner disk. (iii) As in GWL09, inverse Compton scattering is taken as the radiation process, and a Monte Carlo method is used in fitting the spectra of the LH state. However, the code used in GWL09 is modified in this case by considering energy transfer into the jet as shown in Equation (37), and the outer boundary of the corona is fixed at $40M$ rather than at the outer boundary of the closed field lines in GWL09.

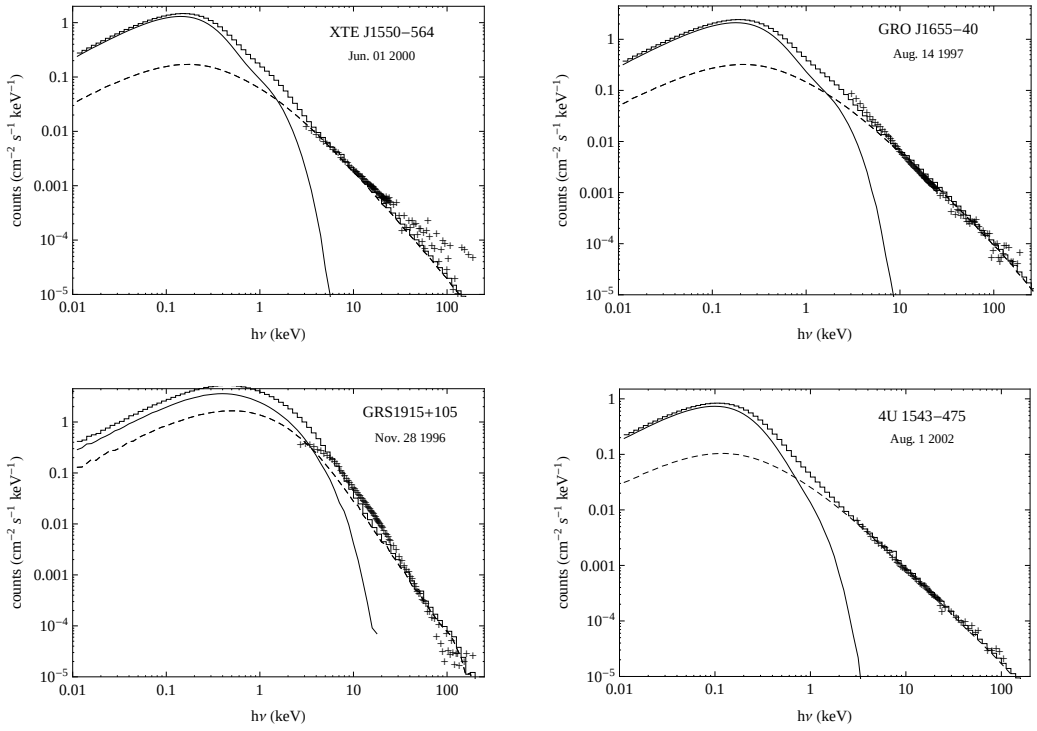

Fig. 7 The spectral profiles of the LH state of four BHXBs are plotted as zigzag lines, which are a superposition of thermal and power law components in solid and dashed lines, respectively.

The fitting is carried out based on the features of the four BHXBs taken from Narayan & McClintock (2012, hereafter NM12) as input parameters as shown in Table 1, and the spectral profiles of the LH state are shown in Figure 7.

It is noticed that the spectral profiles of the LH states of the four BHXBs given in Figure 7 are in good agreement with the observed data given in figure 4.11 of MR06.

4.3 A Constraint on the Magnetic Field Configuration Based on the Relation between Jet Power and X-ray Luminosity

The relation between jet power and X-ray luminosity (hereafter RJPXL) in BHXBs was first proposed by Fender et al. (2003), and it reads

$$L_{\rm J} = A_{\rm steady} L_{\rm X}^{0.5}\,, \tag{38}$$

where the coefficient $A_{\rm steady}$ varies between 6×10^{-3} and 0.3 (FBG04; Malzac et al. 2004).

As is well known, the evolution of the LH state in one outburst of BHXBs can be depicted in the X-ray hardness-intensity diagram (HID) as given by FBG04, and RJPLX implies that the jet power correlates with the X-ray luminosity in a non-linear way. Since this relation is deduced from observations, we can regard it as a constraint on the magnetic field configuration of our model.

Table 2 Describing the Relation between Jet Power and X-ray Luminosity in the LH State

BHXBs	Parameters					
GRO J1655-40	$\dot{m}_{\rm in}$	0.035	0.04	0.045	0.05	0.055
	$r_{\rm out}$	1000	10.22	7.49	6.36	5.67
	$L_{\rm X}$	0.01359	0.01604	0.01884	0.02176	0.02468
	$L_{\rm J}$	0.02238	0.02431	0.02636	0.02833	0.03016
	$P_{\rm BZ}/P_{\rm BP}$	0.97	1.07	1.16	1.25	1.34
4U 1543-475	$\dot{m}_{\rm in}$	0.005	0.0055	0.006	0.0065	0.007
	$r_{\rm out}$	1000	11.31	8.00	6.63	5.82
	$L_{\rm X}$	0.004908	0.005622	0.006423	0.007239	0.008094
	$L_{\rm J}$	0.004187	0.004481	0.004786	0.005087	0.005378
	$P_{\rm BZ}/P_{\rm BP}$	1.46	1.57	1.66	1.74	1.83

In our model, $L_{\rm J}$ is regarded as $P_{\rm jet}$ given by Equation (27), and the values of the related parameters are listed in Table 2, in which the leftmost values of $L_{\rm X}$ are calculated based on the spectral profiles of the LH state given in Figure 7.

In Table 2, the radius $r_{\rm out}$ represents the outer boundary of the BP magnetic field configuration, and the luminosities and accretion rates are defined in terms of Eddington luminosity and Eddington accretion rate, respectively. As shown in Table 2, the radius $r_{\rm out}$ of the outer boundary of the BP magnetic field configuration decreases monotonically with increasing accretion rate $\dot{m}_{\rm in}$, jet power $L_{\rm J}$ and X-ray luminosity $L_{\rm X}$. This result implies that the magnetic field configuration could be related to the state transitions of BHXBs, and this issue will be discussed in the next section.

5 DISCUSSION

In this paper, we propose a corona-disk model for fitting the LH state associated with a steady jet in BHXBs based on the magnetic field configuration that arises from the coexistence of the BZ and BP processes. Some issues related to our model are discussed in this section.

5.1 Transition from LH to VH States in BHXBs

Up to now a consensus on the classification of spectral states of BHXBs has not been reached. It is widely accepted that the spectral states of BHXBs can be reduced to two basic states, i.e., a hard state and a soft state (MR06). As shown in HID, X-ray luminosity always increases after an outburst starts and attains its maximum in the intermediate state during the transition from hard to soft states. However, the properties of the intermediate state remain unclear, and different definitions have been presented, e.g., Steep Power Law (SPL) state by MR06, and very high (VH) state by Esin et al. (1997). Belloni (2006) further classified the intermediate state as hard intermediate (HIM) and soft intermediate (SIM) states. In this paper, we take the intermediate state as the VH state given in NM12, which is associated with the episodic, relativistic jet.

As is well known, state transitions in BHXBs display a variety of variations not only in luminosities but also in some spectral characteristics such as hardness and spectral index. The complexity is particularly attractive in the transition from hard to soft states, with which different remarkable phenomena are associated. A visualized description for the main features of state transitions of BHXBs is given in HID, where the typical spectral evolution traces along a q-shaped pattern and forms a counterclockwise cycle (Belloni 2004; Belloni et al. 2011; Fender & Belloni 2012; FBG04; Fender et al. 2009; Homan & Belloni 2005). Based on HID, the outbursts of BHXBs are generally triggered by a sudden increase of accretion rate from quiescence to the LH state, and the spectra are normally hard with photon index ~ 1.7 being associated with steady jets in LH states, and the jet power is correlated with the X-ray luminosity as $L_{\rm J} \propto L_{\rm X}^{0.5}$. After reaching the peak luminosity, the spectra begin to soften and the jets transit from steady into episodic, indicating the transition from the LH

state to the VH state. After crossing the jet line in HID, the VH state transits to the HS state, calming down with soft spectra without jets. The latest research shows that the HS state is associated with a strong disk wind. Finally, a BHXB returns to its quiescent state with a hard spectrum accompanied by the reappearance of jets (Fender & Belloni 2012; Zhang 2013).

The variation of the X-ray luminosity and spectra is naturally interpreted by the corresponding variation of accretion rate and accretion geometry (Esin et al. 1997; Done 2002, 2010; Done et al. 2007). A series of works on the formation and evolution of the corona give a physical explanation of the spectral state transitions (Liu et al. 2005; Meyer-Hofmeister et al. 2005, 2009, see Zhang 2013 for a review).

However, accretion rate is not the only parameter that governs the state transition of BHXBs, and some phenomena involved cannot be interpreted by only changing accretion rate. For example, state transition from hard to soft occurs at luminosity higher than that in a later reverse transition during one outburst, and this hysteresis cannot be interpreted by the variation of accretion rate (Miyamoto et al. 1995; FBG04; Belloni 2010).

It was suggested by Spruit & Uzdensky (2005) that the size of the central magnetic flux bundle can be identified with the second parameter for determining X-ray spectral states of BHXBs and the presence of relativistic outflows. Very recently, King et al. (2012) pointed out that the magnetic field might be primarily toroidal in the soft state, but primarily poloidal in the hard state. In fact, both the accumulation of the magnetic flux in the inner disk and the change between toroidal and poloidal magnetic fields can be regarded as evolution of the magnetic field configuration. Thus, we suggest that the magnetic field configuration on the accretion disk could be regarded as the second parameter for governing the state transition of BHXBs.

This viewpoint is strengthened by the constraint of RJPXL on the outer boundary of the BP magnetic field configuration as shown in Table 2. The correlation of magnetic field configurations with the transition from LH to VH states is illustrated from the bottom-right to top-left panels in

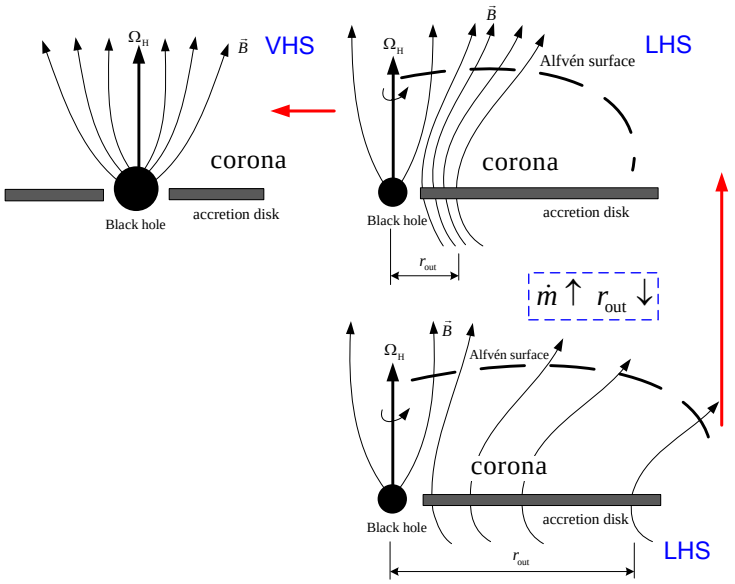

Fig. 8 A schematic drawing of magnetic field configurations in transition from the LH state to the VH state in BHXBs.

Figure 8, in which the outer boundary of the BP magnetic field configuration decreases monotonically with the increasing accretion rate $\dot{m}_{\rm in}$, $L_{\rm J}$ and $L_{\rm X}$ for the validity of RJPXL in LH states of BHXBs given by Equation (38), and the VH state appears as all large-scale poloidal magnetic fields are carried onto the BH as shown by the top-left panel in Figure 8.

The scenario of evolution of magnetic field configuration is also helpful for understanding the correlation of jet power with BH spin, which has been addressed by a number of authors (Meier 1999; McKinney & Gammie 2004; Hirose et al. 2004; De Villiers et al. 2005; Hawley & Krolik 2006; Li et al. 2008; Wu et al. 2011).

Recently, Fender et al. (2010, hereafter FGR10) pointed out that there is no evidence for any correlation between the jet power and the BH spin based on the reported measurements of BH spin and jet power for BHXBs. On the contrary, it was shown in NM12 that the 5-GHz radio flux of transient ballistic jets in BHXBs correlates with the BH spin estimated via the continuum-fitting method, and they pointed out this represents the first direct evidence of jets powered by energy from BH spin.

According to our model, the BZ power is not dominant over the BP power in the LH state corresponding to the magnetic field configuration with large outer boundary radius $r_{\rm out}$, but it gradually becomes dominant over the BP power in the transition from LH to VH states with decreasing $r_{\rm out}$ as shown in Figure 8. It is the magnetic field concentrated on the BH horizon that results in the jet power being proportional to the square of BH spin in the VH state. In addition, the transient ballistic jet in the VH state can be interpreted by invoking the kink instability related to the BZ process (Wang et al. 2006). Therefore by invoking the variation of the large-scale magnetic field configuration, we can resolve the debate between FGR10 and NM12 on the issue of jet power and BH spin in BHXBs.

5.2 Energy Conversion in Launching a Jet and Corona Current

In our model, energy is released from two sources: (i) rotational energy from a spinning BH via the BZ process and (ii) rotational energy from the disk via the accretion process in the BP process. Energy release and conversion are illustrated in Figure 9.

Energy release and conversion are outlined in Figure 9. It is shown that two energy sources (gravitational potential energy of accreting matter and rotational energy of a BH) give rise to two types of energy output from a BH system, i.e., radiation via the accretion process and jet power via the BZ and BP processes are included. Obviously, both magnetic field and rotational energy of a BH arise from the accretion process, so the accretion process is essential for the BZ process.

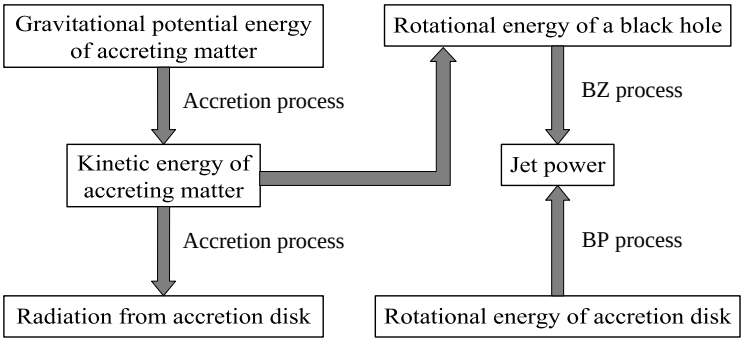

Fig. 9 A block diagram showing energy release and conversion in the accretion disk with the BZ and BP processes.

Regarding energy conversion in the jet, we introduce the corona current, which is required by continuity of current flowing on the disk as shown in Figure 3. Similarly, the corona current is also essential for energy conversion in the BZ jet, which is required by continuity of current flowing on the stretched horizon of a spinning BH (Thorne et al. 1986).

In addition, corona current could be related to the following issues. (i) Strengthening the toroidal magnetic field, which is essential for Poynting flux near the disk surface as shown in Figure 3; (ii) an alternative way of enhancing corona temperature in the form of Joule heating; (iii) an alternative way of exchanging energy between disk and corona. We shall discuss these issues in our future work.

5.3 Advantages and Disadvantages of This Model

Compared to the widely believed model (ADAF), the advantages of our model are related to launching a jet and its application to fitting LH states in BHXBs, which are summarized as follows.

(i) Required by the energy conversion from Poynting flux to the kinetic energy flux in the jet from the accretion disk, coronal current flowing across the magnetic surfaces is naturally introduced in this model. The corona current is essential for continuity of current flowing on the accretion disk, which is crucial for launching a steady jet via the BP process.

(ii) Based on energy conversion in the jet and the work done by magnetic torque exerted on a disk current and corona current, we construct a large-scale magnetic field configuration on the disk for launching a jet, and the LH state is fitted by invoking the accretion process with the coexistence of the BZ and BP processes.

(iii) Based on the above magnetic field configuration, we discuss the relative importance of BZ to BP powers in terms of a few parameters constrained by observational and theoretical considerations, and apply this result to fit the LH state associated with a steady jet.

(iv) Required by the validity of RJPXL, we find that the outer boundary of the BP magnetic field decreases monotonically with the increasing jet power and X-ray luminosity in LH states, and this implies that the magnetic field configuration could be regarded as the second parameter for governing the transition from hard to soft states in BHXBs.

On the other hand, there exist some disadvantages with this model, which are given as follows.

(i) Although the corona current is introduced based on some reasonable consideration, we have not presented a detailed analysis of it, such as how the corona current is distributed in the corona, how it interacts with the disk, how it affects the radiation or spectrum, etc.

(ii) Only inverse Compton scattering is taken into account for the mechanism that produces radiation in fitting the spectra of LH states in order to have a simplified model. As a matter of fact, synchrotron radiation or SSC might be important in fitting. Likewise, we did not consider the contribution of the jet to the radiation.

(iii) We fail to discuss hysteresis in the state transition of some BHXBs, which involves a higher luminosity in the transition from hard to soft spectral states and a lower one at the reverse transition from soft to hard spectral states. Although an explanation has been given by the disk evaporation model (e.g. Meyer-Hofmeister et al. 2005), the physics behind hysteresis remains elusive.

We hope to overcome the above disadvantages and modify this model in future work.

Acknowledgements We are very grateful to the anonymous referee for his (or her) helpful comments on the manuscript. This work is supported by the National Basic Research Program of China (973 Program, No. 2009CB824800) and the National Natural Science Foundation of China (No. 11173011).

Appendix A: DERIVATION OF EQUATION (25)

C02 gives the mass loss rate in the jet from unit surface area of a disk as follows,

$$\dot{m}_{\rm jet} = \frac{(B_{\rm d}^{\rm P})^2}{4\pi}(r_{\rm d}\Omega_{\rm d})^{\alpha}\frac{\gamma_{\rm j}^{\alpha}}{(\gamma_{\rm j}^2-1)^{\frac{\alpha+1}{2}}}\,. \tag{A.1}$$

According to Equation (17) and the context, we have

$$\dot{M}_{\rm jet} = 4\pi r_{\rm d}\dot{m}_{\rm jet} = r_{\rm d}(B_{\rm d}^{\rm P})^2(r_{\rm d}\Omega_{\rm d})^{\alpha}\frac{\gamma_{\rm j}^{\alpha}}{(\gamma_{\rm j}^2-1)^{\frac{\alpha+1}{2}}}\,. \tag{A.2}$$

Combining Equations (17) and (22), we have

$$B_{\rm d}^{\rm P} = B_{\rm in}\left(\frac{r_{\rm d}}{r_{\rm in}}\right)^{s-2} = \sqrt{\frac{\dot{M}_{\rm in}}{\alpha_{\rm m}r_{\rm H}^2}}\left(\frac{r_{\rm d}}{r_{\rm in}}\right)^{s-2}\,. \tag{A.3}$$

Incorporating Equations (A.2), (A.3) and (17), we have

$$\frac{1}{\alpha_{\rm m}r_{\rm H}^2}\left(\frac{r_{\rm d}}{r_{\rm in}}\right)^{s-2}\frac{r_{\rm in}^2}{s}(r_{\rm d}\Omega_{\rm d})^{\alpha} = \frac{(\gamma_{\rm j}^2-1)^{\frac{\alpha+1}{2}}}{\gamma_{\rm j}^{\alpha}}\,, \tag{A.4}$$

and Equation (25) is the dimensionless form of Equation (A.4).

References

Belloni, T. 2004, Nuclear Physics B Proceedings Supplements, 132, 337
Belloni, T. 2006, Advances in Space Research, 38, 2801
Belloni, T. M. 2010, in Lecture Notes in Physics, vol. 794, ed. T. Belloni (Berlin: Springer Verlag), 53
Belloni, T. M., Motta, S. E., & Muñoz-Darias, T. 2011, Bulletin of the Astronomical Society of India, 39, 409
Bisnovatyi-Kogan, G. S., & Ruzmaikin, A. A. 1976, Ap&SS, 42, 401
Blandford, R. D., & Begelman, M. C. 1999, MNRAS, 303, L1
Blandford, R. D., & Payne, D. G. 1982, MNRAS, 199, 883 (BP82)
Blandford, R. D., & Znajek, R. L. 1977, MNRAS, 179, 433
Cao, X. 2002, MNRAS, 332, 999 (C02)
Contopoulos, J. 1995, ApJ, 450, 616
Contopoulos, I., & Kazanas, D. 1998, ApJ, 508, 859
De Villiers, J.-P., Hawley, J. F., Krolik, J. H., & Hirose, S. 2005, ApJ, 620, 878
Doeleman, S. S., Fish, V. L., Schenck, D. E., et al. 2012, Science, 338, 355
Done, C. 2002, Royal Society of London Philosophical Transactions Series A, 360, 1967
Done, C. 2010, arXiv: 1008.2287
Done, C., Gierliński, M., & Kubota, A. 2007, A&A Rev., 15, 1
Esin, A. A., McClintock, J. E., & Narayan, R. 1997, ApJ, 489, 865
Esin, A. A., Narayan, R., Cui, W., Grove, J. E., & Zhang, S.-N. 1998, ApJ, 505, 854
Esin, A. A., McClintock, J. E., Drake, J. J., et al. 2001, ApJ, 555, 483
Fender, R. P., Gallo, E., & Jonker, P. G. 2003, MNRAS, 343, L99
Fender, R. P., Belloni, T. M., & Gallo, E. 2004, MNRAS, 355, 1105 (FBG04)
Fender, R. P., Homan, J., & Belloni, T. M. 2009, MNRAS, 396, 1370
Fender, R. P., Gallo, E., & Russell, D. 2010, MNRAS, 406, 1425 (FGR10)
Fender, R., & Belloni, T. 2012, Science, 337, 540

Gan, Z.-M., Wang, D.-X., & Lei, W.-H. 2009, MNRAS, 394, 2310 (GWL09)
Ghosh, P., & Abramowicz, M. A. 1997, MNRAS, 292, 887
Hawley, J. F., & Krolik, J. H. 2006, ApJ, 641, 103
Hirose, S., Krolik, J. H., De Villiers, J.-P., & Hawley, J. F. 2004, ApJ, 606, 1083
Homan, J., & Belloni, T. 2005, Ap&SS, 300, 107
King, A. L., Miller, J. M., Raymond, J., et al. 2012, ApJ, 746, L20
Lee, H. K., Wijers, R. A. M. J., & Brown, G. E. 2000, Phys. Rep., 325, 83
Li, Y., Wang, D.-X., & Gan, Z.-M. 2008, A&A, 482, 1
Liu, B. F., Meyer, F., & Meyer-Hofmeister, E. 2005, A&A, 442, 555
Liu, B. F., Taam, R. E., Meyer-Hofmeister, E., & Meyer, F. 2007, ApJ, 671, 695
Livio, M., Ogilvie, G. I., & Pringle, J. E. 1999, ApJ, 512, 100
Livio, M. 2002, Nature, 417, 125
Lubow, S. H., Papaloizou, J. C. B., & Pringle, J. E. 1994, MNRAS, 268, 1010
Lynden-Bell, D. 1996, MNRAS, 279, 389
MacDonald, D., & Thorne, K. S. 1982, MNRAS, 198, 345
Malzac, J., Merloni, A., & Fabian, A. C. 2004, MNRAS, 351, 253
Mayer, M., & Pringle, J. E. 2007, MNRAS, 376, 435
McClintock, J. E., & Remillard, R. A. 2006, in Compact Stellar X-ray Sources, eds. W. H. G. Lewin, & M. van der Klis (Cambridge: Cambridge Univ. Press), 157 (MR06)
McKinney, J. C., & Gammie, C. F. 2004, ApJ, 611, 977
Meier, D. L. 1999, ApJ, 522, 753
Merloni, A., & Fabian, A. C. 2002, MNRAS, 332, 165
Meyer-Hofmeister, E., Liu, B. F., & Meyer, F. 2005, A&A, 432, 181
Meyer-Hofmeister, E., Liu, B. F., & Meyer, F. 2009, A&A, 508, 329
Miller, J. M., Homan, J., & Miniutti, G. 2006a, ApJ, 652, L113
Miller, J. M., Homan, J., Steeghs, D., et al. 2006b, ApJ, 653, 525
Miyamoto, S., Kitamoto, S., Hayashida, K., & Egoshi, W. 1995, ApJ, 442, L13
Moderski, R., Sikora, M., & Lasota, J. P. 1997, in Relativistic Jets in AGNs, eds. M. Ostrowski, M. Sikora, G. Madejski, & M. Begelman, 110
Narayan, R., & McClintock, J. E. 2012, MNRAS, 419, L69 (NM12)
Novikov, I. D., & Thorne, K. S. 1973, in Black Holes (Les Astres Occlus), eds. C. Dewitt, & B. S. Dewitt, 343 (Routledge)
Reis, R. C., Miller, J. M., & Fabian, A. C. 2009, MNRAS, 395, L52
Reis, R. C., Fabian, A. C., & Miller, J. M. 2010, MNRAS, 402, 836
Spruit, H. C. 1996, in NATO ASIC Proc. 477: Evolutionary Processes in Binary Stars, eds. R. A. M. J. Wijers, M. B. Davies, & C. A. Tout, 249 (arXiv:astro-ph/9602022)
Spruit, H. C. 2010, in Lecture Notes in Physics, 794, ed. T. Belloni, 233 (Berlin: Springer Verlag) (arXiv:0804.3096)
Spruit, H. C., & Uzdensky, D. A. 2005, ApJ, 629, 960
Thorne, K. S., Price, R. H., & MacDonald, D. A. 1986, Black Holes: The Membrane Paradigm (New Haven, CT: Yale Univ. Press)
Wang, D. X., Xiao, K., & Lei, W. H. 2002, MNRAS, 335, 655
Wang, D.-X., Lei, W.-H., & Ye, Y.-C. 2006, ApJ, 643, 1047
Wu, Q., Cao, X., & Wang, D.-X. 2011, ApJ, 735, 50
Yuan, F., Cui, W., & Narayan, R. 2005, ApJ, 620, 905
Zhang, H., Yuan, F., & Chaty, S. 2010, ApJ, 717, 929
Zhang, S.-N. 2013, Frontiers of Physics (arXiv:1302.5485)